Mechanisms of Insulin Resistance in Primary and Secondary Nonalcoholic Fatty Liver

Tomas Jelenik,[1,2] Kirti Kaul,[1,2] Gilles Séquaris,[1,2] Ulrich Flögel,[3] Esther Phielix,[1,2] Jörg Kotzka,[2,4] Birgit Knebel,[2,4] Pia Fahlbusch,[2,4] Tina Hörbelt,[2,4] Stefan Lehr,[2,4] Anna Lena Reinbeck,[1] Dirk Müller-Wieland,[5] Irene Esposito,[6] Gerald I. Shulman,[7] Julia Szendroedi,[1,2,8] and Michael Roden[1,2,8]

Nonalcoholic fatty liver disease is associated with hepatic insulin resistance and may result primarily from increased hepatic de novo lipogenesis (PRIM) or secondarily from adipose tissue lipolysis (SEC). We studied mice with hepatocyte- or adipocyte-specific SREBP-1c overexpression as models of PRIM and SEC. PRIM mice featured increased lipogenic gene expression in the liver and adipose tissue. Their selective, liver-specific insulin resistance was associated with increased C18:1-diacylglycerol content and protein kinase Cε translocation. SEC mice had decreased lipogenesis mediated by hepatic cholesterol responsive element–binding protein and featured portal/lobular inflammation along with total, whole-body insulin resistance. Hepatic mitochondrial respiration transiently increased and declined with aging along with higher muscle reactive oxygen species production. In conclusion, hepatic insulin resistance originates from lipotoxicity but not from lower mitochondrial capacity, which can even transiently adapt to increased peripheral lipolysis. Peripheral insulin resistance is prevented during increased hepatic lipogenesis only if adipose tissue lipid storage capacity is preserved.

Nonalcoholic fatty liver (NAFL) diseases (NAFLDs) affect one-third of the adult population and range from increased hepatocellular triglyceride (TG) deposition (NAFL, steatosis) and inflammation (nonalcoholic steatohepatitis [NASH]) to cirrhosis (1). Although insulin resistance (IR) tightly associates with NAFLD, the underlying mechanisms remain largely unclear. Selective hepatic IR, characterized by disturbed insulin-mediated suppression of hepatic glucose output but intact stimulation of lipogenesis, may, in contrast to total hepatic IR, contribute to the complex relationships by inducing lipogenic programing and systemic hyperlipidemia (2).

Elevated hepatic TG deposition results mainly from intrahepatic de novo lipogenesis (DNL) (primary NAFL [PRIM]) or from uptake and esterification of fatty acids from sources such as adipose tissue lipolysis and dietary intake (secondary NAFL [SEC]) (3,4). Approximately 60% of total hepatic TG arose from nonesterified fatty acids (NEFAs), 26% from DNL, and 15% from diet in patients with NAFLD (5); moreover, DNL was elevated in the fasting state without diurnal variation. Although a feature of human NAFL (6), hepatic DNL does not necessarily lead to IR (7). Likewise, hepatic IR developed in some (8,9) but not all animal models of PRIM (10,11). However, augmented fatty acid flux to the liver (12) and/or peripheral IR (13) may lead to SEC and hepatic IR.

Several cellular abnormalities could explain IR observed in different forms of NAFL. First, increased accumulation of lipotoxins—such as diacylglycerol (DAG), which activate novel protein kinase C (PKC), or ceramides, which upon Toll-like receptor 4 (TLR4)/fetuin A stimulation inactivate Akt—impairs insulin signaling (3,14). Second, alterations in mitochondrial function could contribute to the development of both NAFL and IR (15). Reduced hepatic energy metabolism correlates with IR, hyperglycemia, and hepatic

[1]Institute for Clinical Diabetology, German Diabetes Center, Düsseldorf, Germany
[2]German Center for Diabetes Research, München-Neuherberg, Germany
[3]Department of Molecular Cardiology, Medical Faculty, Heinrich-Heine University Düsseldorf, Düsseldorf, Germany
[4]Institute for Biochemistry and Pathobiochemistry, German Diabetes Center, Düsseldorf, Germany
[5]Department of Internal Medicine I, University Hospital Aachen, Aachen, Germany
[6]Institute of Pathology, Heinrich-Heine University Düsseldorf, Düsseldorf, Germany
[7]Departments of Internal Medicine and Cellular & Molecular Physiology, Howard Hughes Medical Institute, Yale University School of Medicine, New Haven, CT
[8]Department of Endocrinology and Diabetology, Medical Faculty, Heinrich-Heine University Düsseldorf, Düsseldorf, Germany

lipids (16,17). Recent studies have challenged this concept by reporting transiently increased mitochondrial respiration in human NAFL but impaired mitochondrial efficiency and production of reactive oxygen species (ROS) in NASH (18).

We tested the hypotheses that 1) in PRIM, increased hepatic DNL gives rise to lipotoxins, which would induce IR in the liver, whereas 2) in SEC, lipid flow from adipose tissue would enhance hepatic mitochondrial oxidation, promote inflammation, and also lead to redistribution of lipids to peripheral tissues, thereby causing whole-body IR. We used mouse models of primary, genetically induced NAFL resulting from increased hepatic DNL (19) and of secondary NAFL secondarily resulting from ectopic lipid deposition (20), which allow comparing the effects of both pathways separately.

RESEARCH DESIGN AND METHODS

Animals
Female transgenic mice, 18 and 36 weeks of age, with NAFL resulting from PRIM-specific (19) or SEC-specific (20) overexpression of the SREBP-1c, and matched C57Bl6 controls (CON) were maintained under pathogen-free conditions on a 12-h light-dark cycle and received rodent diet (Ssniff M-Z Extrudat, 4.5% fat; SSNIFF Spezialdiäten GmbH, Soest, Germany) and water ad libitum. All experiments were performed according to the guidelines for the care and use of animals (GV-SOLAS [Society for Laboratory Animal Science]) and approved by the local council of animal care in line with the requirements of the German Animal Protection Act.

Indirect Calorimetry
Mice were individually housed and placed in an eight-chamber indirect calorimetry system (PhenoMaster; TSE Systems, Bad Homburg, Germany). After 24 h of acclimatization, respiratory quotient, physical activity, and food and water intake were simultaneously analyzed for 48 h (12).

DNL in Primary Hepatocytes
DNL was quantified ex vivo in primary hepatocytes obtained by liver perfusion and by measuring the ^{14}C-acetate lipid incorporation as described previously (21).

Hyperinsulinemic-Euglycemic Clamps
Clamps were performed in conscious mice 3–5 days after the surgical placement of a silicon catheter into the right jugular vein. Rates of endogenous glucose production (EGP) and whole-body R_d were assessed using D-[6,6-[2]H$_2$]glucose (98% enriched; Cambridge Isotope Laboratories, Andover, MA) (12).

High-Resolution Respirometry
Oxygen consumption rates were measured in fresh liver and gastrocnemius muscle using the Oxygraph-2k (Oroboros Instruments, Innsbruck, Austria) (12). Liver (~50 mg of the left lobe) was permeabilized mechanically (22) and muscle (~30 mg) chemically with saponin (23). Defined respiratory states were obtained with substrates for β-oxidation–linked and tricarboxylic acid (TCA) cycle–linked respiration (Fig. 5A and D).

Whole-Body and Tissue Lipid Content by MRI and Spectroscopy
Experiments were performed in anesthetized mice (1.5% isoflurane) using a Bruker Avance[III] 9.4-T 89-mm bore MR spectrometer, Bruker microimaging unit (Micro 2.5), and Paravision 5.1 as operating software. Abdominal ^{1}H MRIs and spectra were taken from a 30-mm saw resonator, while acquisition of ^{1}H MR spectra from tibialis anterior or soleus muscle was performed with a 10-mm saddle coil. Analyses of abdominal fat, hepatic lipid content, and intramyocellular lipids were performed as previously described (24,25). The degree of total fatty acid saturation was assessed with ^{1}H MR, which has been previously validated (26).

H$_2$O$_2$ Emission
H$_2$O$_2$ emission was continuously monitored in permeabilized liver and soleus muscle using Amplex Red (18) and the Oxygraph-2k Fluorescence Module (Oroboros Instruments). Two protocols at state 4o respiration (10 μg/mL oligomycin) were used: 1) malate (2 μmol/L), glutamate (5 μmol/L), and succinate (stepwise 0.05–2.5 mmol/L) and 2) malate (2 μmol/L) and octanoyl-carnitine (0.2 mmol/L). Rotenone (0.1 μmol/L) was used to inhibit complex I electron backflow and antimycin A (2.5 μmol/L) to inhibit complex III and maximize H$_2$O$_2$ emission. Calibration was performed with H$_2$O$_2$.

Hepatic Lipid Peroxidation and Systemic Oxidative Stress
Tissue concentrations of thiobarbituric acid reactive substances (TBARS) were measured fluorometrically (BioTek, Bad Friedrichshall, Germany) (12). Static oxidation reduction potential (sORP) and antioxidant capacity were determined as markers of systemic oxidative stress in plasma using the RedoxSYS (Luoxis Diagnostics, Inc., Englewood, CO) (27).

Mitochondrial Density
Mitochondrial DNA copy number (mtDNA) was quantified with real-time PCR (ABI Prism 7000; Applied Biosystems, Darmstadt, Germany) and expressed as the ratio of mitochondrial (NADH dehydrogenase 1) to nuclear (lipoprotein lipase) DNA (12).

Citrate synthase activity was assessed spectrophotometrically (Citrate Synthase Assay Kit; Sigma-Aldrich, St. Louis, MO) and expressed per protein.

Liver Histology
Harvested liver tissues were cryopreserved, and sections were stained with hematoxylin and eosin and Fat Red according to standard conditions. Histological scoring of NASH criteria was performed by an experienced pathologist (I.E.) blinded to the experimental setup (28).

Insulin Signaling
Mice were injected intraperitoneally with insulin 1 unit/kg body weight or saline and sacrificed after 10 min, and tissues were snap frozen in liquid nitrogen.

RNA and Protein Analyses
RNA and protein extraction and quantifications were performed by real-time RT-PCR and Western blots as

previously described (12). Membrane and cytosol fractions were prepared with differential centrifugation (29).

Laboratory Analyses

Serum insulin was measured with Ultrasensitive Mouse Insulin ELISA kit (Mercodia, Uppsala, Sweden). D-[6,6-^{2}H$_2$]glucose enrichment in deproteinized plasma was quantified with gas chromatography–mass spectrometry (Agilent Technologies, Waldbronn, Germany) after derivatization of glucose to pentaacetate. Serum TG, cholesterol (Roche/Hitachi, Roche Diagnostics, Mannheim, Germany), and NEFAs (Wako Chemicals GmbH, Neuss, Germany) were assessed photometrically (12). Cytokines were analyzed in serum and liver homogenates using the Bio-Plex Pro Mouse Cytokine 23-plex Assay (Bio-Rad Laboratories, Hercules, CA). Hepatic cytokines were expressed per protein content.

Calculations and Statistical Analyses

R_d was calculated by Steele's single-pool non–steady-state equations (30). EGP is given as the difference between R_d and the glucose infusion rate. Data are presented as means $\pm$ SD in the text and tables and as means $\pm$ SEM in figures. Groups were compared using the Bonferroni test or nonparametric unpaired t test (Mann-Whitney) with Hochberg post hoc analysis. P values of <0.05 were considered to indicate statistically significant differences.

RESULTS

Increased Hepatic Lipid Accumulation and Impaired Lipid Oxidation but Differences in Whole-Body Lipid Distribution and Hepatic Inflammation in PRIM and SEC Mice

Body weight was unchanged in PRIM mice, but increased by 10% in SEC compared with CON at both ages (Fig. 1A). Energy expenditure and food intake were unchanged during light (fasted) and dark (fed) periods (Supplementary Table 1). Unlike CON, PRIM and SEC exhibited high respiratory quotients during light versus dark phases, indicating impaired metabolic flexibility (i.e., ability to switch from glucose to lipid oxidation) (Fig. 1B).

Compared with CON, 36-week-old PRIM and SEC had larger livers and greater accumulation of lipid droplets (Fig. 1D), confirmed by 87% and 191% higher hepatic lipids, assessed with ^{1}H MRS (Fig. 1F). Histology revealed portal and lobular inflammation without hepatocellular ballooning or fibrosis in SEC (Supplementary Fig. 1A). Interleukin-6 and tumor necrosis factor-α decreased in the liver of SEC at both ages (Supplementary Figs. 1B and 6). Circulating cytokines were unchanged among the groups (Supplementary Fig. 7). Livers of PRIM showed upregulated expression of fatty acid synthase (Fas), a DNL gene under the transcriptional control of SREBP-1c (Fig. 1G). Livers of SEC had increased stearoyl-CoA desaturase (Scd1) expression, associated with higher monounsaturated fatty acids (Supplementary Fig. 1C). The expression of carbohydrate-responsive element–binding protein (Chrebp) was decreased (Fig. 1G). Only SEC had higher intramyocellular lipids along with increased Fas and Scd1 expression (Fig. 1H and J).

Visceral and subcutaneous fat depots were increased by 225% and 275% in PRIM but decreased by 56% and 90% in SEC, respectively (Fig. 1I). This associated with changes in the expression of Chrebp, Fas, and Scd1 in adipose tissue (Fig. 1I and K). The 18-week-old mice featured similar mRNA expression data (data not shown).

Increased Hepatic DNL in PRIM but Not SEC Mice

DNL in primary hepatocytes was quantified by measuring ^{14}C-acetate incorporation into lipids under low-/high-glucose and low-/high-insulin conditions. Hepatocytes exhibited the typical hexagonal shape with one or two nuclei and higher lipid droplet content in PRIM and SEC (Fig. 2A). There was a linear increase in ^{14}C-acetate of lipid fraction in all genotypes and studied conditions (Fig. 2B). DNL was markedly increased under all metabolic conditions in PRIM but not in SEC compared with CON (Fig. 2C).

### Liver-Specific IR in PRIM Mice but Whole-Body IR in SEC Mice

At 18 weeks, fasting blood glucose (FBG) and insulin levels were unchanged in PRIM but higher in SEC compared with CON (Fig. 3A and B). Insulin but not glucose remained higher in SEC also in the fed state (Supplementary Fig. 2A and B). Basal EGP followed a similar pattern as FBG (Fig. 3C), and both parameters positively correlated across all mice (Pearson correlation, $r = 0.383$; $P < 0.05$, $n = 37$). Insulin-induced suppression of EGP was 47% and 65% lower in PRIM and SEC, respectively, indicating hepatic IR compared with CON (Fig. 3E). Insulin-stimulated R_d was 76% and 74% lower only in SEC, indicating peripheral IR (Fig. 3F). From 18 weeks to 36 weeks, FBG further rose while insulin levels declined in SEC (Fig. 3A and B).

We analyzed insulin signaling after intraperitoneal injection of insulin or saline. In line with clamps, 18-week-old PRIM and SEC had blunted hepatic Akt cytosolic-to-membrane translocation and lower phosphorylated (p) Akt-Thr308 (Fig. 3G). pAkt-Ser473 was lower only in SEC. In skeletal muscle, SEC exhibited no insulin-stimulated GLUT4 cytosolic-to-membrane translocation, pAkt-Thr308, or pAkt-Ser473, in line with muscle IR (Fig. 3H). Similar results were observed in 36-week-old mice (Supplementary Fig. 2C and D).

We further assessed adipose tissue insulin sensitivity from plasma NEFA in 6-h fasted mice after intraperitoneal insulin or saline injection. Fasting NEFAs were comparable among groups. At 36 weeks, insulin decreased plasma NEFA by 45% in CON and by 56% in PRIM, but not in SEC (Fig. 3D). Likewise, insulin suppression of NEFA was lower in SEC compared with CON mice during the clamp (Supplementary Fig. 2E), indicating impaired suppression of lipolysis by insulin. Similar results were observed at 18 weeks (data not shown).

The DAG-PKC Pathway Associates With Hepatic IR in PRIM and With Muscle IR in SEC Mice

In livers of 18-week-old mice, total cytosolic and membrane DAG were increased in SEC but unchanged in PRIM compared
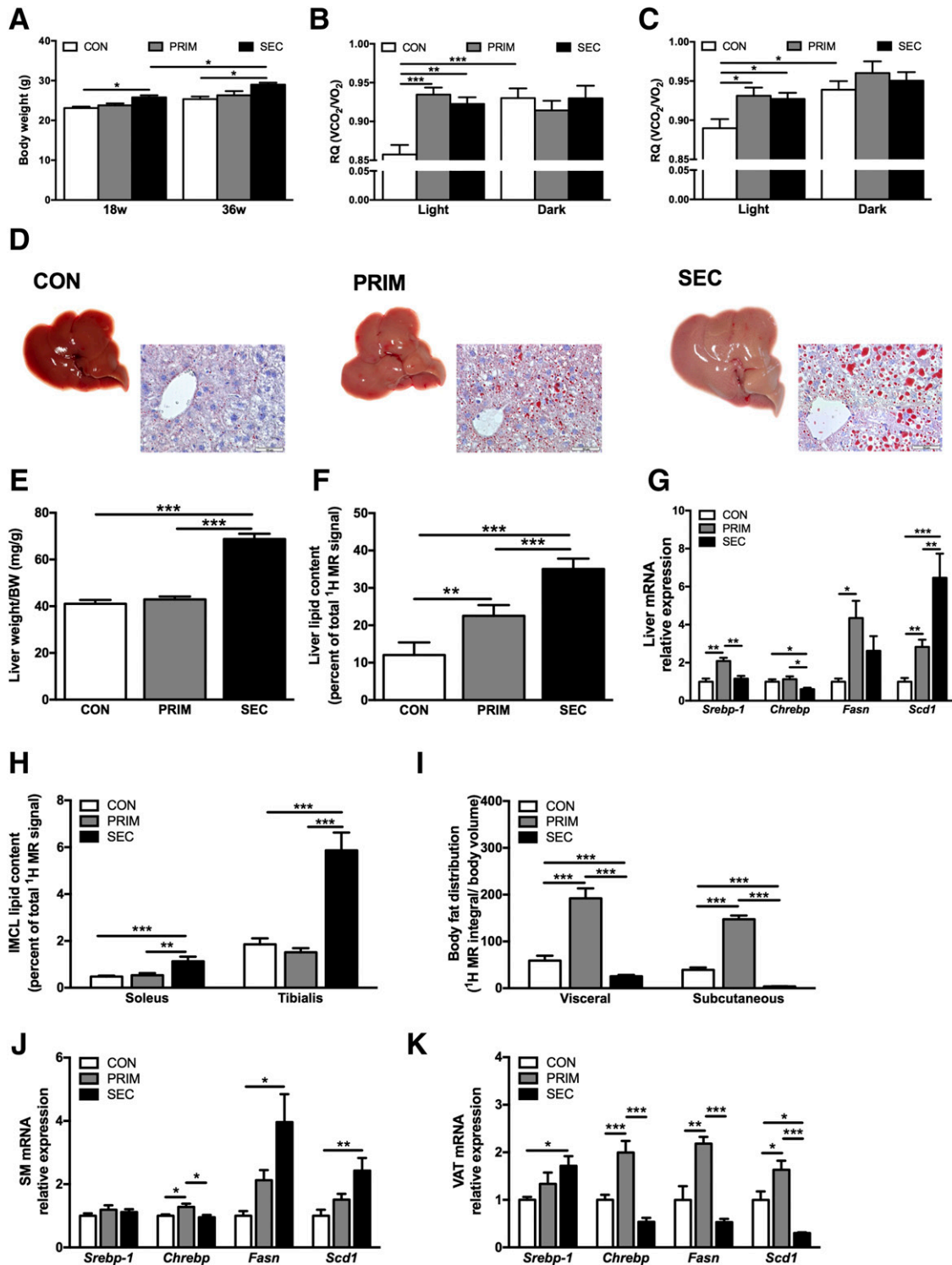
Figure 1—Whole-body and tissue-specific lipid metabolism in PRIM and SEC mice. Body weight (*A*) and respiratory quotients (RQ) during light (fasted) and dark (fed) periods in 18-week-old (*B*) and 36-week-old (*C*) mice measured with indirect calorimetry (*n* = 6–10 per group). *D*: Representative images of the livers and visualization of neutral lipids and lipid droplet morphology with Oil Red O staining in the liver sections from 36-week-old mice. Scale bars = 50 μm. Liver weight–to–body weight (BW) ratio (*E*) and liver lipid content measured with ^{1}H MRS (*F*) in 36-week-old mice (*n* = 7–9 per group). *G*: Relative expression of *Srebp-1*, *Chrebp*, *Fasn*, and *Scd1* lipogenic genes in the livers of 36-week-old mice assessed with quantitative RT-PCR (*n* = 5–7 per group). *H*: Intramyocellular lipids (IMCL) measured in soleus and tibialis skeletal muscles measured with ^{1}H MRS in 36 week-old mice (*n* = 7–9 per group). *I*: Distribution of visceral and subcutaneous adipose tissue depots measured with MRI in 36-week-old mice (*n* = 7–9 per group). Relative expression of *Srebp-1*, *Chrebp*, *Fasn*, and *Scd1* lipogenic genes in the gastrocnemius skeletal muscle (SM) (*J*) and epididymal visceral adipose tissue (VAT) (*K*) of 36-week-old mice assessed with quantitative RT-PCR (*n* = 5–7 per group). All data are presented as mean ± SEM. *$P < 0.05$, **$P < 0.01$, ***$P < 0.001$ by two-way ANOVA (*A*–*C*) or one-way ANOVA (*E*–*K*) with Bonferroni correction.
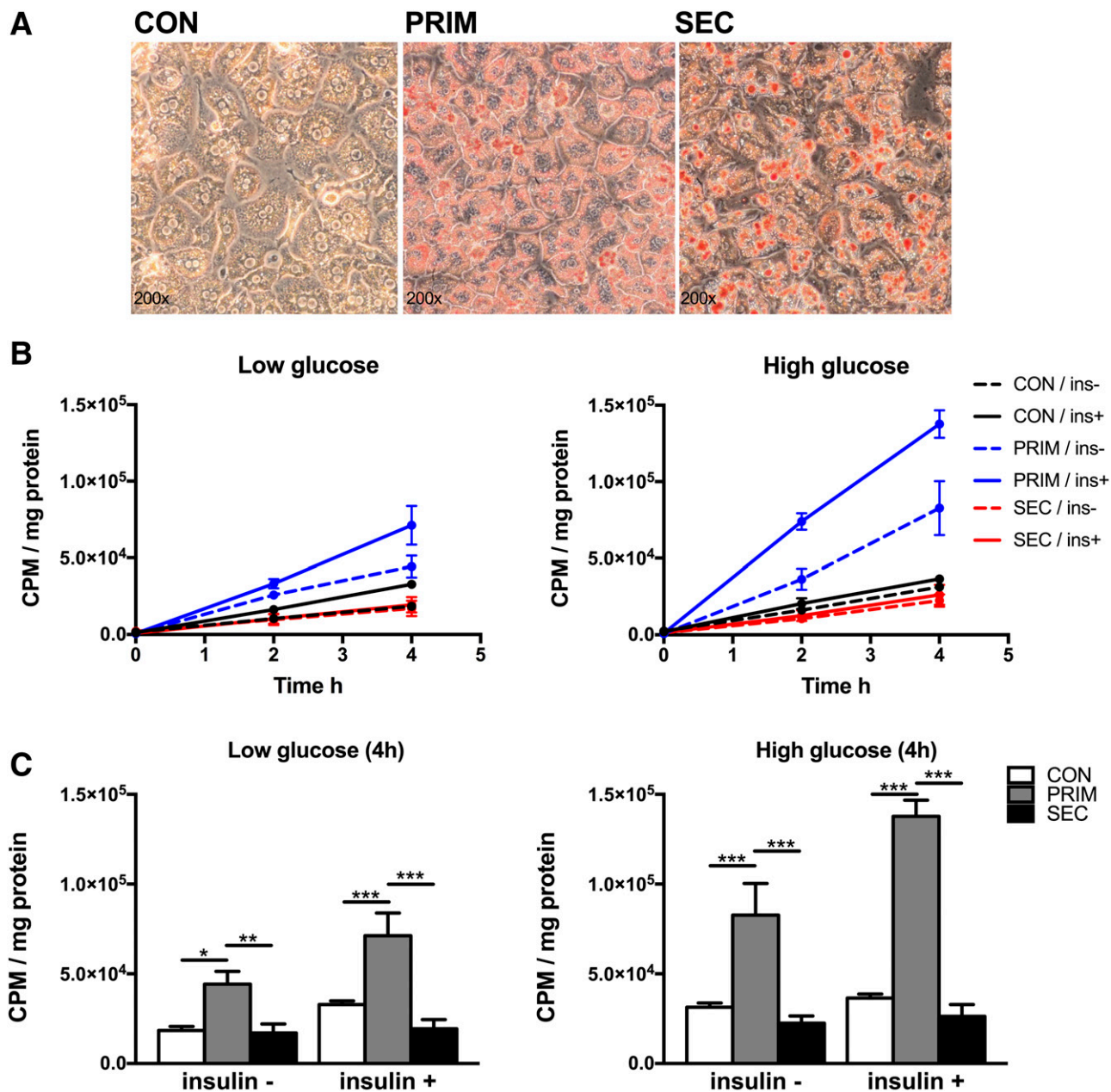
Figure 2—High rates of hepatic DNL in primary hepatocytes. A: Representative photomicrographs of lipid droplets visualized with Oil Red O staining in primary hepatocytes from CON, PRIM, and SEC mice. B: Incorporation of ^{14}C-acetate at 0, 2, and 4 h after incubation, without or with 100 nmol/L insulin (ins), and with low (5.5 mmol/L) or high (25 mmol/L) glucose. C: Comparison of rates of ^{14}C-acetate lipid incorporation at 4 h after incubation with substrates. Data are presented as mean ± SEM. *$P < 0.05$, **$P < 0.01$, ***$P < 0.001$ by two-way ANOVA with Bonferroni correction (C). CPM, counts per min.

with CON (Supplementary Fig. 3A and B). Several species of cytosolic DAG, containing at least one unsaturated fatty acid, gradually increased in PRIM and SEC (Fig. 4A). Membrane DAG C18:1/C16:0 increased only in SEC (Supplementary Fig. 4A). Protein content of PKCε, a negative regulator of insulin receptor kinase activity (31), markedly increased only in PRIM (Fig. 4C). However, phosphorylated insulin receptor substrate 2 (pIRS2)-Tyr gradually decreased in PRIM and SEC (Fig. 4D). Total ceramides were unchanged in PRIM compared with CON and decreased in

SEC compared with PRIM (Supplementary Fig. 3C). C24:1 ceramides increased only in PRIM and C20:0 ceramides in both PRIM and SEC, whereas C22:0, C24:1, and C24:0 ceramides decreased in SEC compared with CON (Fig. 4E). Most of the ceramide species decreased in 36-week-old PRIM and SEC compared with CON (Fig. 4F).

In skeletal muscles of 18-week-old mice, total cytosolic and membrane DAG increased in SEC, but not in PRIM (Supplementary Fig. 3D and E). Both cytosolic and
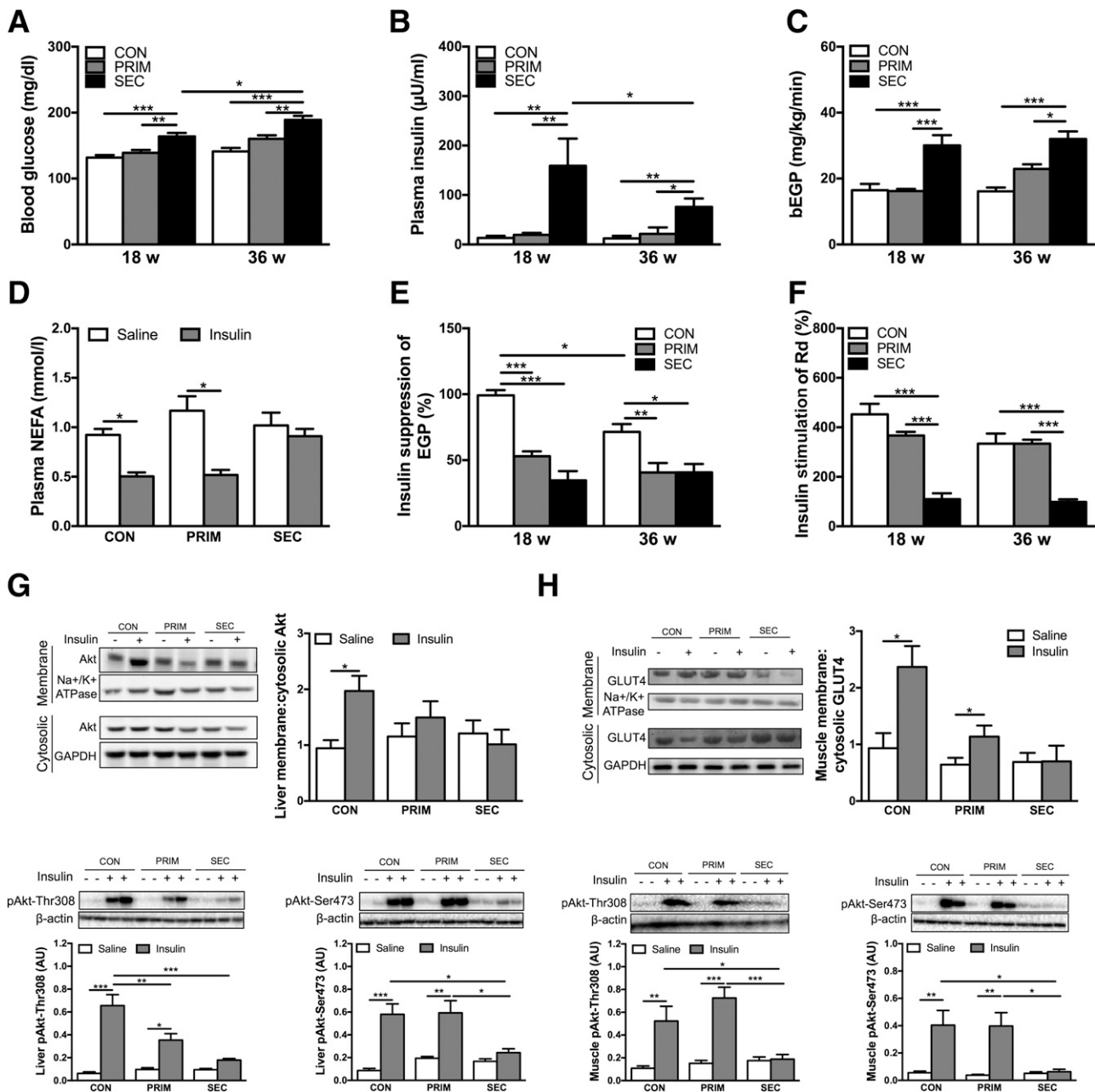
Figure 3—Increased hepatic DNL is associated with insulin resistance in the liver but not in peripheral tissues. Blood glucose (A) and plasma insulin (B) levels measured in 6-h fasted mice (n = 7–8 per group). C: Basal EGP (bEGP) assessed in vivo using D-[6,6-^{2}H$_2$]glucose infusion in 6 h fasted mice (n = 5–8 per group). D: NEFA measured in the plasma of 36-week-old mice from blood collected 10 min after saline or insulin (1 unit/kg) intraperitoneal injection in 6-h fasted mice (n = 7–9 per group). Insulin suppression of EGP (E) and insulin stimulation of R_d (F) assessed in vivo with hyperinsulinemic-euglycemic clamp combined with D-[6,6-^{2}H$_2$]glucose infusion in 6-h fasted mice (n = 5–8 per group). Cytosolic-to-membrane translocation of Akt, pAkt-Thr308, and pAkt-Ser473 in the liver (G) and GLUT4, pAkt-Thr308, and pAkt-Ser473 in the gastrocnemius muscle (H) of 36-week-old mice. AU, arbitrary units. Tissues were collected 10 min after saline or insulin (1 unit/kg) intraperitoneal injection in 6-h fasted mice (n = 6–8 per group). Representative Western blots are shown. Data are presented as mean ± SEM. *P < 0.05, **P < 0.01, ***P < 0.001 by two-way ANOVA with Bonferroni correction (A–C, E, and F) or multiple t test with Sidak-Bonferroni correction (D, G, and H).

membrane C18:1/C16:0-, C18:1/C18:1-, and C18:1/C18:2-containing DAG increased solely in SEC (Fig. 4G and Supplementary Fig. 4C). PKCθ was higher in SEC compared with CON (Fig. 4I), and inhibitory phosphorylation of IRS1 at Ser1101 (pIRS1-Ser1101) was higher in SEC than in CON and PRIM (Fig. 4J). Total ceramides were unchanged in PRIM and SEC (Supplementary Fig. 3F), and ceramide C18:0 was even decreased in SEC (Fig. 4K).

At 36 weeks, only DAG C18:1/18:1 remained increased in SEC (Fig. 4H and Supplementary Fig. 4D). Differences in PKCθ and pIRS1-Ser1101 remained comparable to those in 18-week-old mice.
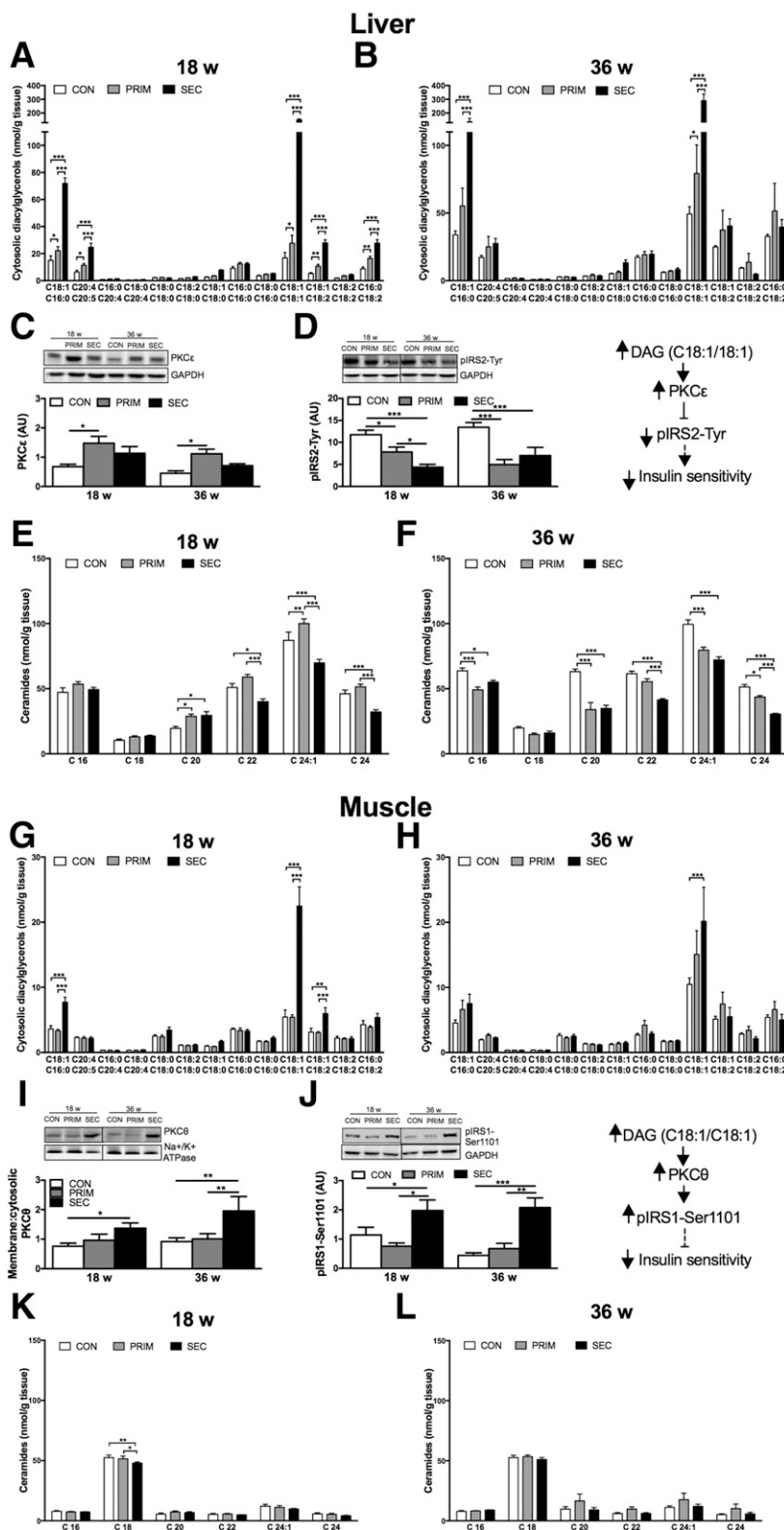
Figure 4—Accumulation of specific DAGs but not ceramides associates with insulin resistance in the liver of PRIM and muscle of SEC mice. Fatty acid composition of cytosolic DAGs in the liver of 6-h fasted 18-week-old (*A*) and 36-week-old (*B*) mice. Relative protein expression of PKCε (*C*) and pIRS2-Tyr (*D*) in the liver assessed with Western blots. Fatty acid composition of ceramides in the liver of 18-week-old (*E*) and 36-week-old (*F*) mice. Fatty acid composition of cytosolic DAGs in the muscle of 18-week-old (*G*) and 36-week-old (*H*) mice. Relative protein expression of PKCθ (*I*) and pIRS1-Ser1101 (*J*) in the muscle assessed with Western blots. Fatty acid composition of ceramides in the muscle of 18-week-old (*K*) and 36-week-old (*L*) mice. AU, arbitrary units. Data are presented as mean ± SEM (*n* = 6–7 per group). *$P < 0.05$, **$P < 0.01$, ***$P < 0.001$ by two-way ANOVA with Bonferroni correction.
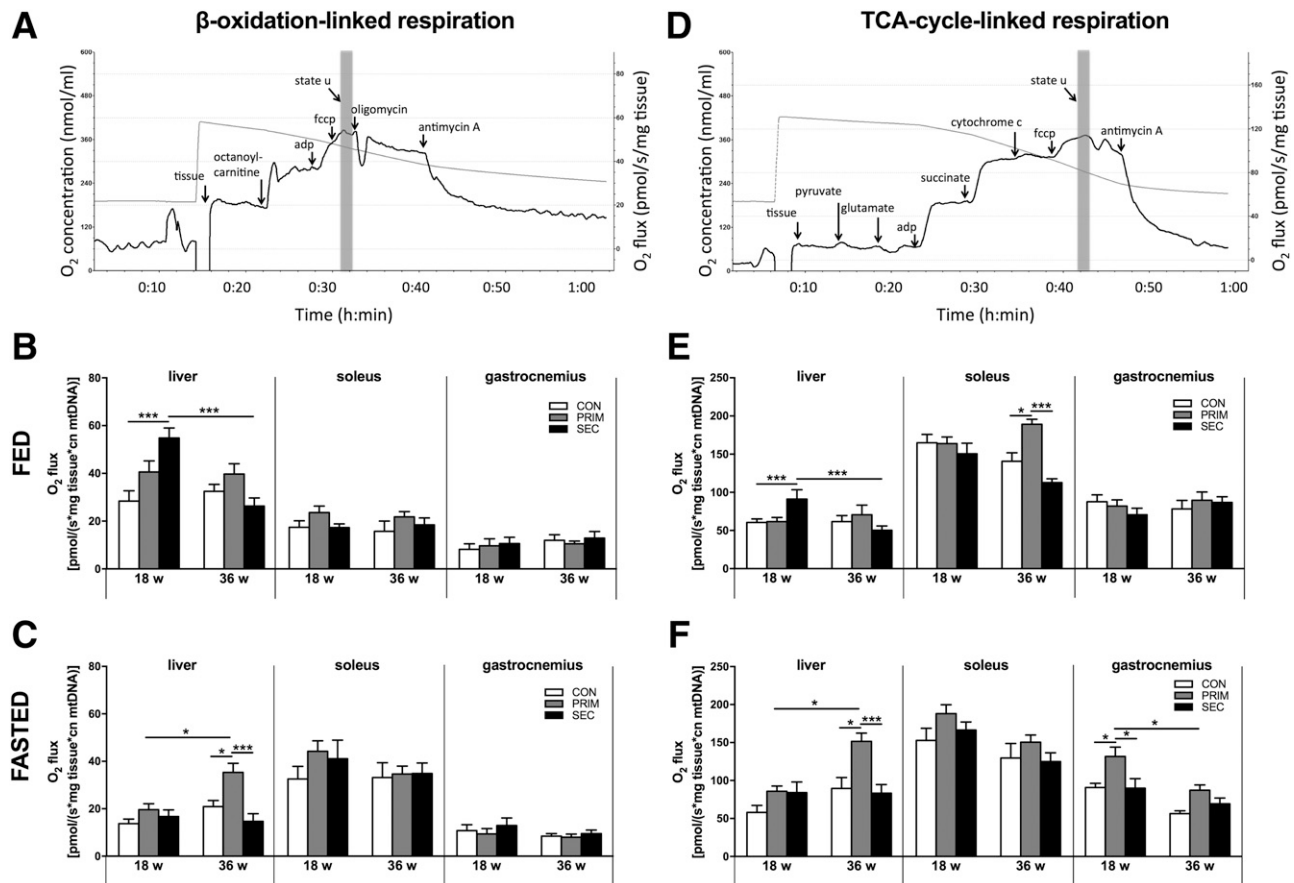
Figure 5—Mitochondrial oxidative capacity in the liver, soleus, and gastrocnemius muscles of PRIM and SEC mice. Specific protocols were used to monitor oxygen consumption during mitochondrial respiration linked to the β-oxidation cycle (A) and TCA cycle (D). Maximal respiratory capacity is given as fluoro-carbonyl cyanide phenylhydrazone (fccp)–driven (state u) respiration (gray column). β-Oxidation–linked maximal respiratory capacity in the fed (B) and fasted (C) states. TCA cycle–linked maximal respiratory capacity in the fed (E) and fasted (F) states. Data are presented as mean ± SEM (n = 6–9 per group). *P < 0.05, ***P < 0.001 by two-way ANOVA with Bonferroni correction. cn, copy number.

Transient Upregulation of Mitochondrial Oxidative Capacity in Livers but Not in Muscles of PRIM and SEC Mice

Maximal respiratory capacity was monitored under fed and fasted conditions. β-Oxidation- and TCA cycle–linked substrates were used, and data are presented as fluoro-carbonyl cyanide phenylhydrazone–driven state u respiration (Fig. 5A and D), normalized to mtDNA, which was comparable between the groups (data not shown). Citrate synthase activity was also comparable among the groups (data not shown).

In the fed state, hepatic β-oxidation–linked respiration was higher in SEC compared with CON at 18 weeks but not at 36 weeks of age (Fig. 5B). It was also increased in 36-week-old fasted PRIM mice (Fig. 5C). Hepatic TCA cycle–linked respiration showed similar results (Fig. 5E and F). In soleus and gastrocnemius, there were no differences in β-oxidation–linked respiration under fed or fasted conditions. However, TCA cycle–linked respiration increased in the gastrocnemius of fasted 18-week-old PRIM mice compared with 36-week-old PRIM as well as age-matched CON

and SEC mice (Fig. 5F). In the fed state, 36-week-old PRIM mice showed higher respiration in the soleus muscle than CON and SEC (Fig. 5E).

Systemic and Muscle-Specific Oxidative Stress Develop Only in SEC Mice After a Long-standing IR

Succinate-stimulated (Fig. 6A) and octanoyl-carnitine–stimulated (Fig. 6C) H_2O_2 emissions were unchanged in the liver. Leak respiration, which is predominantly controlled by the proton leak activity (32) and can be induced by ROS (33), also did not change (Fig. 6B). Hepatic TBARS even decreased in 18-week-old SEC compared with PRIM (Supplementary Fig. 5). In the soleus of 36-week-old SEC, augmented succinate-stimulated H_2O_2 emission (Fig. 6D) was accompanied by higher leak respiration (Fig. 6E). Octanoyl-carnitine–stimulated H_2O_2 emission also increased (Fig. 6F). Dose-response curves showed that H_2O_2 was stimulated by lower succinate concentrations in 36-week-old SEC (Fig. 6G). Also, sORP (27) was higher, whereas antioxidant capacity was lower, in the serum of these mice (Fig. 6H and I). Moreover, sORP positively correlated with
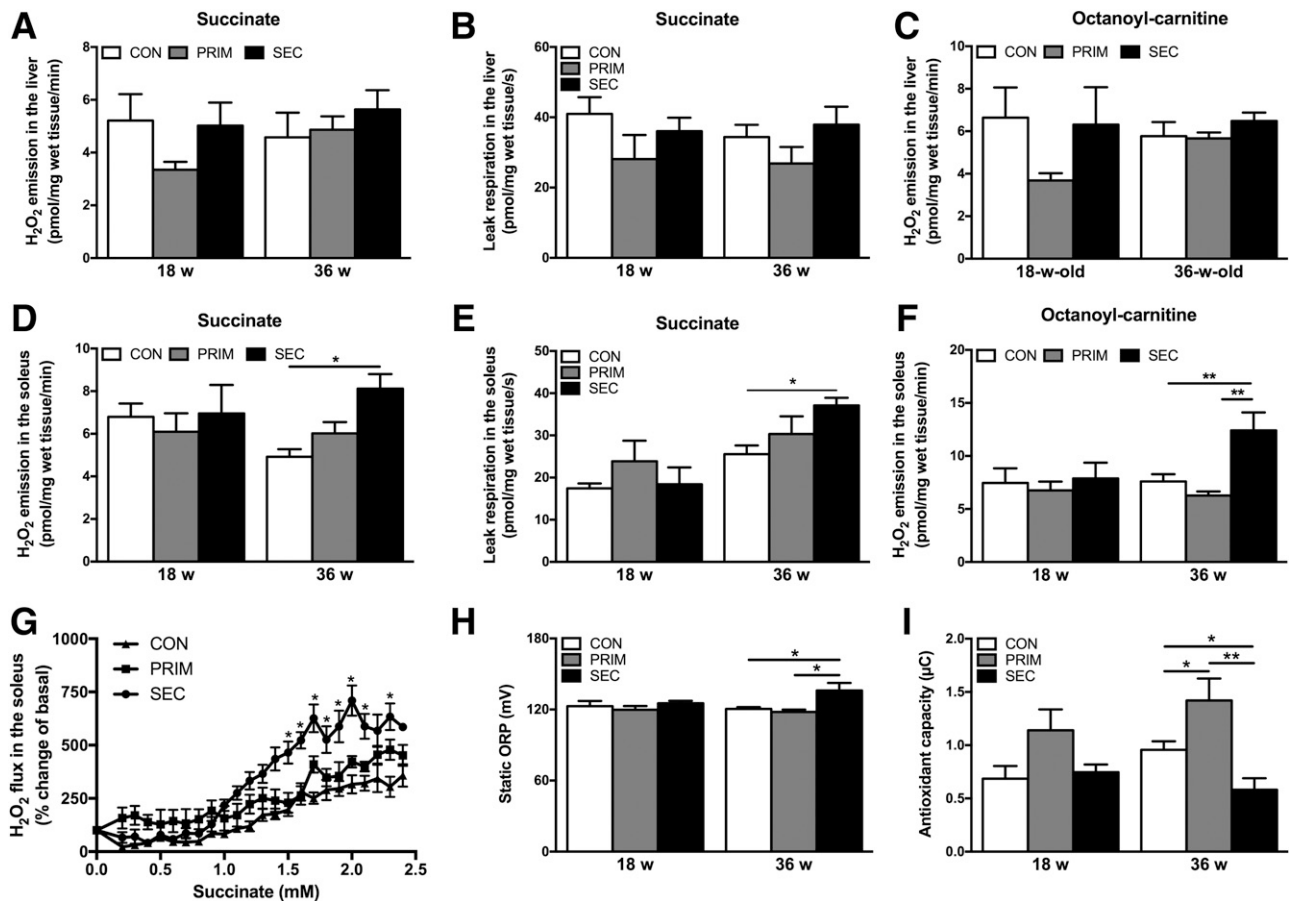
Figure 6—Mitochondrial H_2O_2 emission, proton leak respiration, and systemic oxidative stress in PRIM and SEC mice. Succinate-stimulated H_2O_2 emission (*A*) and leak respiration (*B*) in the liver. *C*: Octanoyl-carnitine–stimulated H_2O_2 emission in the liver. Succinate-stimulated H_2O_2 emission (*D*) and leak respiration (*E*) in the soleus muscle. *F*: Octanoyl-carnitine–stimulated H_2O_2 emission in the soleus muscle. *G*: Dose-response curves of succinate-stimulated H_2O_2 emission in the soleus muscle of 36-week-old mice. Plasma measurements of sORP (*H*) and antioxidant capacity (*I*). Data are presented as mean ± SEM (*n* = 5–6 per group). *$P < 0.05$, **$P < 0.05$ by two-way ANOVA with Bonferroni correction.

the muscle H_2O_2 emission (Pearson correlation, $r = 0.78$; $P < 0.0001$).

DISCUSSION

We found that primary NAFL caused by increased DNL (PRIM) associates with selective hepatic IR, accumulation of 18:1-DAG, and higher PKCε. However, PRIM is prevented from muscle IR along with enhanced ChREBP in adipose tissue (Fig. 7). Secondary NAFL caused by increased adipose-tissue lipolysis (SEC) associates with decreased ChREBP-mediated lipogenesis and results in total hepatic and whole-body IR, followed by oxidative stress as well as portal and lobular inflammation (Fig. 7). Of note, impaired mitochondrial function (i.e., decreased oxidative capacity and/or increased oxidative stress) does not precede IR. Indeed, hepatic mitochondrial oxidative capacity transiently adapts to lipolysis but not intrahepatic lipogenesis.

Liver-specific overexpression of SREBP-1c in PRIM mice resulted in the induction of lipogenic genes *Fas* and *Scd1* along with doubling hepatic lipids. Simultaneously, selective

hepatic IR was demonstrated by the decreased insulin-mediated suppression of EGP and downregulated hepatic insulin signaling. While *Srebp-1c* expression in skeletal muscle and adipose tissue remained unchanged, *Chrebp* expression was increased, followed by increased expression of *Fas* and *Scd1* and lipid accumulation in adipose tissue of PRIM mice. Proper functioning of ChREBP and induction of DNL in adipose tissue has been shown to be crucial for maintaining whole-body insulin sensitivity (34). Furthermore, obese people with increased adipose tissue capacity for lipogenesis are protected from weight gain–induced IR (35). In line, insulin-stimulated glucose disposal and muscle insulin signaling remained comparable to age-matched CON, indicating intact peripheral insulin sensitivity in PRIM mice. Increased *Chrebp* expression and DNL in adipose tissue of PRIM could reflect higher flux of glucose from the IR liver, resulting in clearance of glucose via ortho-topic storage of TG in adipose tissue instead of ectopic accumulation of lipids and their metabolites in skeletal muscle. Indeed, glucose can stimulate ChREBP at the
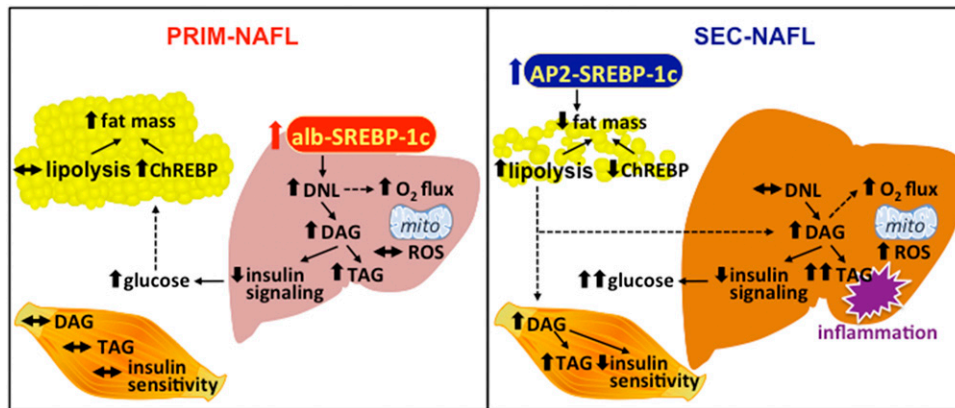
Figure 7—Interplay between glucose and lipid metabolism in the PRIM and SEC models of NAFLD. Liver-specific overexpression of SREBP-1c and increased hepatic DNL in the PRIM mouse model leads to accumulation of DAGs and triacylglycerols (TAG) and development of NAFLD. NAFLD in PRIM associates with decreased insulin signaling and higher hepatic glucose output. On the one hand, mitochondrial oxidative capacity (O_2 flux) is increased under fasted conditions while emission of ROS remains unchanged. ChREBP-mediated lipogenesis in adipose tissue and fat mass are increased, which could protect from hyperglycemia and peripheral IR. On the other hand, SEC mice are characterized by loss of adipose tissue and ectopic lipid (DAG, TAG) accumulation in both liver and skeletal muscle. Moreover, accumulation of extrahepatic lipids in SEC but not intrahepatic lipids in PRIM associates with portal and lobular inflammation of the liver. In SEC, hepatic O_2 flux is increased under fed conditions as well as systemic oxidative stress. Liver and skeletal muscle are both characterized by decreased insulin sensitivity. alb, albumin; AP2, adipocyte P2.

translational level (34) as well as posttranslational level (36). Moreover, glucose could facilitate TG synthesis as a substrate for glycerol-3-phosphate synthesis.

In line with the observation in male mice (20), female SEC mice with adipose tissue–specific overexpression of SREBP-1c also show marked loss of adipose tissue. The development of this lipodystrophic phenotype is still poorly understood. On the one hand, the female SEC mice featured decreased ChREBP-mediated lipogenesis along with impaired insulin-mediated suppression of lipolysis, which could explain the robust loss of adipose tissue. On the other hand, these mice had an almost threefold increase in hepatic lipids and developed whole-body IR, as assessed in vivo as well as ex vivo. Hepatic expression of *Fas* was unchanged, but *Chrebp* decreased, indicating impairment in DNL and the presence of total hepatic IR. However, *Scd1* expression was induced in line with the higher content of total monounsaturated fatty acids, which likely reflects higher uptake of NEFA originating from adipose tissue lipolysis and their subsequent incorporation into hepatic DAG and TG instead of ceramides. Of note, SCD1 and synthesis of monounsaturated fatty acids are required for the production of hepatic cholesterols and TG in mice (37). This is in line with the recent finding that hepatic esterification of fatty acids into TG, unlike DNL, depends on substrate delivery but not insulin action (38). Taken together, hepatic fat originates mostly from augmented intrahepatic DNL in PRIM, but mainly from uptake and esterification of fatty acids originating from lipolysis of extrahepatic tissues in SEC mice.

This study also describes how hepatic and muscle mitochondrial oxidative capacity relate to IR during the development of NAFL. Previous clinical studies in patients with type 2 diabetes suggested that impaired mitochondrial energy metabolism associates with IR and NAFL (17,39).

However, mechanistic studies in rodents reported conflicting results; for example, ablation of mitochondrial biogenesis induced IR (40), whereas knockout of mitochondrial oxidative phosphorylation genes protected against IR (41). Moreover, mitochondrial function was impaired in the livers of *ob/ob* mice (42) and even preceded the development of NAFL and IR in OLETF rats (43) but did not change (44) in diet-induced obesity and IR.

Weight gain–induced NAFL in obese humans associates with an imbalance between hepatic fatty acid availability and disposal (45). NAFLD, which encompasses genetic and lifestyle factors, can result from both pathways of lipid availability (i.e., SREBP-1c–induced DNL as well as increased fatty acid uptake from lipolysis). Most of the TG in the livers of patients with NAFLD derives from NEFA, whereas ~26% results from DNL (5). Our study allows comparison of the effects of NEFA from DNL and lipolysis on mitochondrial function separately by using nonobese PRIM and SEC mice. Hepatic β-oxidation–linked as well as TCA cycle–linked mitochondrial oxidative capacity increased in 36-week-old PRIM in the fasted state. Also, mice with high-fructose diet–induced DNL showed higher rates of mitochondrial respiration and improved mitochondrial efficiency (46). It has been proposed that this could provide energy sources for DNL and gluconeogenesis, which were both increased in the livers of PRIM mice. Furthermore, we found a transient increase in β-oxidation–linked as well as TCA cycle–linked mitochondrial oxidative capacity in the livers of fed 18-week-old SEC mice. Similarly, a high-fat diet, as an exogenous source for hepatic lipids, as in SEC mice with high lipolysis, leads to increased expression of genes responsible for fatty acid oxidation after 4 weeks but not after 10 weeks of dietary intervention (47). We recently showed that postprandial hepatic energy metabolism is

augmented in young, obese humans without diabetes but not in patients with type 2 diabetes (48). Furthermore, hepatic mitochondrial respiration increases in NAFL but decreases when NAFL progresses to NASH (18). The transient increase in mitochondrial function likely reflects an adaptation to a specific threshold of hepatic lipid concentration in obesity, IR, and NAFL, which, however, does not suffice to catabolize lipids and protect from their accumulation. Even more, high respiratory rates associate with augmented oxidative stress and NASH progression (18).

How different lipid sources (i.e., intrahepatic DNL and fatty acid uptake) and other factors contribute to the early development of early NASH (i.e., hepatic inflammation) is currently unknown. On the one hand, the current study shows that PRIM mice with increased DNL did not develop hepatic inflammation, hepatocellular ballooning, or fibrosis. On the other hand, SEC mice, characterized by increased fatty acid uptake, developed mild lobular and portal inflammation at 36 weeks of age, in line with initiation of progressive NAFLD. In animal models with genetically and dietary-induced NAFLD, several stimuli, such as abnormal mitochondrial function with oxidative stress, altered lipid partitioning mediated by NEFA, or hyperinsulinemia, have been discussed as an important second hit causing progression from NAFL to NASH (49). Although muscle and systemic oxidative stress increased in the older SEC mice, hepatic ROS production, lipid peroxidation, mitochondrial coupling, and mitochondrial mass were unchanged in SEC. Thus, these mechanisms unlikely explain the observed changes in mitochondrial respiration and the onset of inflammation in the livers of 36-week-old SEC mice. More likely, accumulation of hepatic lipotoxins, such as DAG, drives hepatic inflammation. Indeed, several pharmacological agents for the treatment of NASH in humans improve lipid metabolism and also have anti-inflammatory effects (50,51).

Mostly unsaturated DAG accumulated in the liver of both PRIM and SEC mice, accompanied by the decrease in activating pIRS2-Tyr phosphorylation. In the livers of obese humans, cytosolic DAG content but not ceramides positively correlated with IR and PKCε activation (29). As shown previously, leptin can reverse IR in SEC mice (52) and hepatic steatosis in another lipodystrophic mouse model by reducing enzymes of DAG synthesis (53). Furthermore, a novel mechanism of hepatic IR, mediated by the accumulation of white adipose tissue–derived acetyl-CoA, has been recently described (54). Because SEC mice are characterized by the impaired suppression of adipose tissue lipolysis, that this mechanism also contributes to their hepatic IR cannot be excluded.

Neither impaired muscle mitochondrial respiration nor increased ROS production is linked to the induction of muscle IR in SEC mice. ROS production as well as high sORP and low antioxidant capacity developed only in older SEC mice. Moreover, muscle IR was accompanied with accumulation of specific DAG, containing at least one C18:1 fatty acid, and with activation of PKCθ and inhibitory pIRS1-Ser1101 phosphorylation in

SEC mice. However, muscle ceramides and plasma fetuin A (data not shown), which have been previously linked to IR (55–57), were both unchanged, probably as a result of increased mRNA expression of Scd1 and lower availability of saturated fatty acids in skeletal muscle of SEC mice. None of these changes were present in the insulin-sensitive muscle of PRIM mice, which, however, displayed a moderate increase in circulating fetuin A. This suggests that fetuin A is dissociated from muscle IR in these experimental models.

Taken together, we have shown that PRIM mice represent a primary NAFL model as a result of increased hepatic DNL characterized by liver-specific selective IR. SEC mice represent a secondary NAFL model because of the accumulation of extrahepatic lipids originating mostly from lipolysis of adipose tissue and are characterized by total hepatic and whole-body IR. Both models exhibited higher rather than impaired hepatic mitochondrial respiration, while the degree of oxidative stress remained unchanged. Accumulation of extrahepatic lipids in SEC, but not intrahepatic lipids in PRIM, associates with portal and lobular inflammation of the liver. Impaired muscle mitochondrial function was present after the development of IR only in SEC mice. Thus, IR in these two different models with NAFL can result not from impaired mitochondrial function but from increased accumulation of specific DAG. The source of hepatic lipids is an important prerequisite for the progression to NASH in lipid-induced NAFLD and IR.

References

1. European Association for the Study of the Liver (EASL); European Association for the Study of Diabetes (EASD); European Association for the Study of Obesity (EASO). EASL-EASD-EASO Clinical Practice Guidelines for the management of nonalcoholic fatty liver disease. J Hepatol 2016;64:1388–1402.

2.   Brown MS, Goldstein JL. Selective versus total insulin resistance: a pathogenic paradox. Cell Metab 2008;7:95–96

3.   Samuel VT, Shulman GI. The pathogenesis of insulin resistance: integrating signaling pathways and substrate flux. J Clin Invest 2016;126:12–22

4.   Saponaro C, Gaggini M, Carli F, Gastaldelli A. The subtle balance between lipolysis and lipogenesis: a critical point in metabolic homeostasis. Nutrients 2015;7: 9453–9474

5.   Donnelly KL, Smith CI, Schwarzenberg SJ, Jessurun J, Boldt MD, Parks EJ. Sources of fatty acids stored in liver and secreted via lipoproteins in patients with nonalcoholic fatty liver disease. J Clin Invest 2005;115:1343–1351

6.   Lambert JE, Ramos-Roman MA, Browning JD, Parks EJ. Increased de novo lipogenesis is a distinct characteristic of individuals with nonalcoholic fatty liver disease. Gastroenterology 2014;146:726–735

7.   Hooper AJ, Adams LA, Burnett JR. Genetic determinants of hepatic steatosis in man. J Lipid Res 2011;52:593–617

8.   Koonen DP, Jacobs RL, Febbraio M, et al. Increased hepatic CD36 expression contributes to dyslipidemia associated with diet-induced obesity. Diabetes 2007;56: 2863–2871

9.   Samuel VT, Liu ZX, Qu X, et al. Mechanism of hepatic insulin resistance in non-alcoholic fatty liver disease. J Biol Chem 2004;279:32345–32353

10.   Monetti M, Levin MC, Watt MJ, et al. Dissociation of hepatic steatosis and insulin resistance in mice overexpressing DGAT in the liver. Cell Metab 2007;6:69–78

11.   Sun Z, Miller RA, Patel RT, et al. Hepatic Hdac3 promotes gluconeogenesis by repressing lipid synthesis and sequestration. Nat Med 2012;18:934–942

12.   Jelenik T, Séquaris G, Kaul K, et al. Tissue-specific differences in the development of insulin resistance in a mouse model for type 1 diabetes. Diabetes 2014; 63:3856–3867

13.   Semple RK, Sleigh A, Murgatroyd PR, et al. Postreceptor insulin resistance contributes to human dyslipidemia and hepatic steatosis. J Clin Invest 2009;119: 315–322

14.   Shulman GI. Ectopic fat in insulin resistance, dyslipidemia, and cardiometabolic disease. N Engl J Med 2014;371:1131–1141

15.   Jelenik T, Roden M. Mitochondrial plasticity in obesity and diabetes mellitus. Antioxid Redox Signal 2013;19:258–268

16.   Schmid AI, Szendroedi J, Chmelik M, Krssák M, Moser E, Roden M. Liver ATP synthesis is lower and relates to insulin sensitivity in patients with type 2 diabetes. Diabetes Care 2011;34:448–453

17.   Szendroedi J, Chmelik M, Schmid AI, et al. Abnormal hepatic energy homeostasis in type 2 diabetes. Hepatology 2009;50:1079–1086

18.   Koliaki C, Szendroedi J, Kaul K, et al. Adaptation of hepatic mitochondrial function in humans with non-alcoholic fatty liver is lost in steatohepatitis. Cell Metab 2015;21:739–746

19.   Knebel B, Haas J, Hartwig S, et al. Liver-specific expression of transcriptionally active SREBP-1c is associated with fatty liver and increased visceral fat mass. PLoS One 2012;7:e31812

20.   Shimomura I, Hammer RE, Richardson JA, et al. Insulin resistance and diabetes mellitus in transgenic mice expressing nuclear SREBP-1c in adipose tissue: model for congenital generalized lipodystrophy. Genes Dev 1998;12:3182–3194

21.   Akie TE, Cooper MP. Determination of fatty acid oxidation and lipogenesis in mouse primary hepatocytes. J Vis Exp 2015:e52982

22.   Kuznetsov AV, Strobl D, Ruttmann E, Königsrainer A, Margreiter R, Gnaiger E. Evaluation of mitochondrial respiratory function in small biopsies of liver. Anal Biochem 2002;305:186–194

23.   Pesta D, Gnaiger E. High-resolution respirometry: OXPHOS protocols for human cells and permeabilized fibers from small biopsies of human muscle. Methods Mol Biol 2012;810:25–58

24.   Szczepaniak LS, Dobbins RL, Stein DT, McGarry JD. Bulk magnetic susceptibility effects on the assessment of intra- and extramyocellular lipids in vivo. Magn Reson Med 2002;47:607–610

25.   Tucci S, Flögel U, Sturm M, Borsch E, Spiekerkoetter U. Disrupted fat distribution and composition due to medium-chain triglycerides in mice with a β-oxidation defect. Am J Clin Nutr 2011;94:439–449

26.   Strobel K, van den Hoff J, Pietzsch J. Localized proton magnetic resonance spectroscopy of lipids in adipose tissue at high spatial resolution in mice in vivo. J Lipid Res 2008;49:473–480

27.   Stagos D, Goutzourelas N, Bar-Or D, et al. Application of a new oxidation-reduction potential assessment method in strenuous exercise-induced oxidative stress. Redox Rep 2015;20:154–162

28.   Bedossa P; FLIP Pathology Consortium. Utility and appropriateness of the fatty liver inhibition of progression (FLIP) algorithm and steatosis, activity, and fibrosis (SAF) score in the evaluation of biopsies of nonalcoholic fatty liver disease. Hepatology 2014;60:565–575

29.   Kumashiro N, Erion DM, Zhang D, et al. Cellular mechanism of insulin resistance in nonalcoholic fatty liver disease. Proc Natl Acad Sci U S A 2011;108: 16381–16385

30.   Steele R. Influences of glucose loading and of injected insulin on hepatic glucose output. Ann N Y Acad Sci 1959;82:420–430

31.   Samuel VT, Liu ZX, Wang A, et al. Inhibition of protein kinase Cepsilon prevents hepatic insulin resistance in nonalcoholic fatty liver disease. J Clin Invest 2007;117: 739–745

32.   Brand MD, Nicholls DG. Assessing mitochondrial dysfunction in cells. Biochem J 2011;435:297–312

33.   Brookes PS. Mitochondrial H(+) leak and ROS generation: an odd couple. Free Radic Biol Med 2005;38:12–23

34.   Herman MA, Peroni OD, Villoria J, et al. A novel ChREBP isoform in adipose tissue regulates systemic glucose metabolism. Nature 2012;484:333–338

35.   Fabbrini E, Yoshino J, Yoshino M, et al. Metabolically normal obese people are protected from adverse effects following weight gain. J Clin Invest 2015;125:787–795

36.   Bricambert J, Miranda J, Benhamed F, Girard J, Postic C, Dentin R. Salt-inducible kinase 2 links transcriptional coactivator p300 phosphorylation to the prevention of ChREBP-dependent hepatic steatosis in mice. J Clin Invest 2010;120: 4316–4331

37.   Miyazaki M, Kim YC, Gray-Keller MP, Attie AD, Ntambi JM. The biosynthesis of hepatic cholesterol esters and triglycerides is impaired in mice with a disruption of the gene for stearoyl-CoA desaturase 1. J Biol Chem 2000;275:30132–30138

38.   Vatner DF, Majumdar SK, Kumashiro N, et al. Insulin-independent regulation of hepatic triglyceride synthesis by fatty acids. Proc Natl Acad Sci U S A 2015;112: 1143–1148

39.   Pérez-Carreras M, Del Hoyo P, Martín MA, et al. Defective hepatic mitochondrial respiratory chain in patients with nonalcoholic steatohepatitis. Hepatology 2003;38: 999–1007

40.   Vianna CR, Huntgeburth M, Coppari R, et al. Hypomorphic mutation of PGC-1beta causes mitochondrial dysfunction and liver insulin resistance. Cell Metab 2006; 4:453–464

41.   Pospisilik JA, Knauf C, Joza N, et al. Targeted deletion of AIF decreases mitochondrial oxidative phosphorylation and protects from obesity and diabetes. Cell 2007;131:476–491

42.   Holmström MH, Iglesias-Gutierrez E, Zierath JR, Garcia-Roves PM. Tissue-specific control of mitochondrial respiration in obesity-related insulin resistance and diabetes. Am J Physiol Endocrinol Metab 2012;302:E731–E739

43.   Rector RS, Thyfault JP, Uptergrove GM, et al. Mitochondrial dysfunction precedes insulin resistance and hepatic steatosis and contributes to the natural history of non-alcoholic fatty liver disease in an obese rodent model. J Hepatol 2010;52: 727–736

44.   Ciapaite J, Bakker SJ, Van Eikenhorst G, et al. Functioning of oxidative phosphorylation in liver mitochondria of high-fat diet fed rats. Biochim Biophys Acta 2007: 1772:307–316

45.   Fabbrini E, Tiemann Luecking C, Love-Gregory L, et al. Physiological mechanisms of weight gain-induced steatosis in people with obesity. Gastroenterology 2016;150:79–81.e72

46. Crescenzo R, Bianco F, Falcone I, Coppola P, Liverini G, Iossa S. Increased hepatic de novo lipogenesis and mitochondrial efficiency in a model of obesity induced by diets rich in fructose. Eur J Nutr 2013;52:537–545

47. Chan MY, Zhao Y, Heng CK. Sequential responses to high-fat and high-calorie feeding in an obese mouse model. Obesity (Silver Spring) 2008;16:972–978

48. Fritsch M, Koliaki C, Livingstone R, et al. Time course of postprandial hepatic phosphorus metabolites in lean, obese, and type 2 diabetes patients. Am J Clin Nutr 2015;102:1051–1058

49. Takahashi Y, Soejima Y, Fukusato T. Animal models of nonalcoholic fatty liver disease/nonalcoholic steatohepatitis. World J Gastroenterol 2012;18:2300–2308

50. Cusi K. Treatment of patients with type 2 diabetes and non-alcoholic fatty liver disease: current approaches and future directions. Diabetologia 2016;59:1112–1120

51. Gastaldelli A, Harrison SA, Belfort-Aguilar R, et al. Importance of changes in adipose tissue insulin resistance to histological response during thiazolidinedione treatment of patients with nonalcoholic steatohepatitis. Hepatology 2009;50:1087–1093

52. Shimomura I, Hammer RE, Ikemoto S, Brown MS, Goldstein JL. Leptin reverses insulin resistance and diabetes mellitus in mice with congenital lipodystrophy. Nature 1999;401:73–76

53. Cortés VA, Cautivo KM, Rong S, Garg A, Horton JD, Agarwal AK. Leptin ameliorates insulin resistance and hepatic steatosis in Agpat2-/- lipodystrophic mice independent of hepatocyte leptin receptors. J Lipid Res 2014;55:276–288

54. Perry RJ, Camporez JP, Kursawe R, et al. Hepatic acetyl CoA links adipose tissue inflammation to hepatic insulin resistance and type 2 diabetes. Cell 2015;160:745–758

55. Holland WL, Bikman BT, Wang LP, et al. Lipid-induced insulin resistance mediated by the proinflammatory receptor TLR4 requires saturated fatty acid-induced ceramide biosynthesis in mice. J Clin Invest 2011;121:1858–1870

56. Goustin AS, Derar N, Abou-Samra AB. Ahsg-fetuin blocks the metabolic arm of insulin action through its interaction with the 95-kD β-subunit of the insulin receptor. Cell Signal 2013;25:981–988

57. Pal D, Dasgupta S, Kundu R, et al. Fetuin-A acts as an endogenous ligand of TLR4 to promote lipid-induced insulin resistance. Nat Med 2012;18:1279–1285